



This is a repository copy of *Survival of environmental DNA in sediments: mineralogic control on DNA taphonomy*.

White Rose Research Online URL for this paper:

<https://eprints.whiterose.ac.uk/205969/>

Version: Published Version

Article:

Freeman, C.L. orcid.org/0000-0002-6326-1211, Dieudonné, L., Agbaje, O.B.A. et al. (4 more authors) (2023) Survival of environmental DNA in sediments: mineralogic control on DNA taphonomy. Environmental DNA. ISSN 2637-4943

<https://doi.org/10.1002/edn3.482>

Reuse

This article is distributed under the terms of the Creative Commons Attribution (CC BY) licence. This licence allows you to distribute, remix, tweak, and build upon the work, even commercially, as long as you credit the authors for the original work. More information and the full terms of the licence here:

<https://creativecommons.org/licenses/>


Takedown

If you consider content in White Rose Research Online to be in breach of UK law, please notify us by emailing eprints@whiterose.ac.uk including the URL of the record and the reason for the withdrawal request.



eprints@whiterose.ac.uk
<https://eprints.whiterose.ac.uk/>

Survival of environmental DNA in sediments: Mineralogic control on DNA taphonomy

C. L. Freeman¹ | L. Dieudonné^{2,3} | O. B. A. Agbaje² | M. Žure² | J. Q. Sanz² | M. Collins^{2,4} | K. K. Sand² 

¹Department of Materials Science and Engineering, The University of Sheffield, Sheffield, UK

²Globe Institute, University of Copenhagen, Copenhagen, Denmark

³École nationale supérieure de chimie de Mulhouse, Université de Haute-Alsace, Mulhouse, France

⁴Department of Archaeology, University of Cambridge, Cambridge, UK

Correspondence

K. K. Sand, Globe Institute, University of Copenhagen, Copenhagen, Denmark.
Email: kks@sund.ku.dk

Funding information

Danmarks Grundforskningsfond, Grant/Award Number: DNRF128; Engineering and Physical Sciences Research Council, Grant/Award Number: EP/R018820/1; H2020 Marie Skłodowska-Curie Actions, Grant/Award Number: 892889; Natur og Univers, Det Frie Forskningsråd, Grant/Award Number: 8123-00003A; Villum Fonden, Grant/Award Number: 00025352

Abstract

The extraction of environmental DNA (eDNA) from sediments is providing groundbreaking views of past ecosystems and biodiversity. Despite this rich source of information, it is still unclear which sediments favor preservation and why. Here, we used atomic force microscopy and molecular dynamics simulations to explore the DNA-mineral interaction to assess how mineralogy and interfacial geochemistry play a role in the preservation of environmental DNA on mineral substrates. We demonstrate that mineral composition, surface topography, and surface charge influence DNA adsorption behavior as well as preservation. Modeling and experimental data show that DNA damage can be induced by mineral binding if there is a strong driving force for adsorption. The study shows that knowledge of the mineralogical composition of a sediment and the environmental conditions can be useful for assessing if a deposit is capable of storing extracellular DNA and to what extent the DNA would be preserved. Our data adds to the understanding of eDNA taphonomy and highlights that, for some mineral systems, fragmented DNA may not represent old DNA.

KEYWORDS

atomic force microscopy, calcite, DNA preservation, eDNA, interfacial geochemistry, MD simulations

1 | INTRODUCTION

Arguably the most significant breakthrough in the analysis of environmental DNA (eDNA) is the ability to recover DNA sequences (Haile et al., 2007; Hofreiter et al., 2003). The perspectives of harvesting eDNA are vast and include the possibility of using eDNA sources to recover biodiversity in a contemporary setting or across time and space (Giguet-Covex et al., 2019; Pedersen et al., 2016). In situations where fossils are absent, eDNA from sedimentary sources has, for example, been employed to detect the presence of archaic humans (Slon et al., 2017), record animal

processing (Seersholm et al., 2016) and establish past ecosystems (Kjær et al., 2022). While DNA suspended in the water column degrades within a few weeks (Dejean et al., 2011; Thomsen et al., 2012), eDNA associated with sediments can persist for up to 2 Ma (Kjær et al., 2022). Current research efforts aim to identify promising sediments and locations for sedimentary ancient DNA (sedaDNA) studies, taking into account degradation from dynamic biological, physical, and chemical factors (Levy-Booth et al., 2007). However, the potential of mineral surfaces to retain and preserve DNA is often overlooked. Despite the role minerals can play in DNA preservation, very little is known about how DNA associates

This is an open access article under the terms of the [Creative Commons Attribution](https://creativecommons.org/licenses/by/4.0/) License, which permits use, distribution and reproduction in any medium, provided the original work is properly cited.

© 2023 The Authors. *Environmental DNA* published by John Wiley & Sons Ltd.

with mineral surfaces, which mineral species are most prone to preserving DNA, and the reasons behind such interactions. The amount of preserved organic material in a particular sediment is instead used as a qualitative indicator for DNA preservation, and hence organic-rich sediments are often the focus of sedaDNA studies. If we have a better understanding of the role minerals play in DNA retention, transport, and preservation (here: taphonomy), we can broaden the range of sediments and environments studied and achieve biodiversity estimates at higher spatial resolutions. By gaining a deeper understanding of how minerals affect DNA retention, transport, and preservation (referred to here as taphonomy), researchers can expand the variety of sediments and environments under study, leading to biodiversity estimates with greater spatial resolution. A comprehensive knowledge of factors influencing taphonomy can also enhance the reach of modern-day sedaDNA studies, facilitating more strategic sediment sampling to glean information about specific catchments.

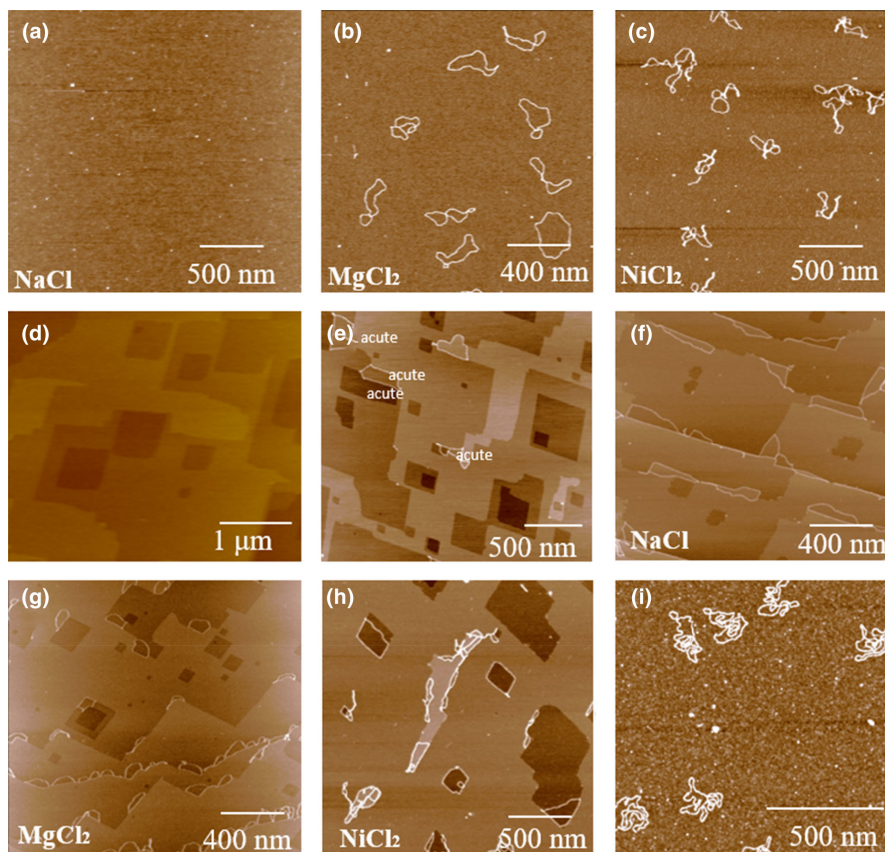
Sediments exhibit a diverse mineralogical composition. Grounded in interfacial geochemical principles, this diversity can significantly impact DNA–mineral associations, especially when combined with varying environmental conditions. The composition and structure of minerals give rise to variations in surface charges and densities. These, in turn, influence the bond strength of adsorbed DNA, its adsorption behavior, and its capacity. Most mineral surfaces undergo changes in surface charge based on pH. For instance, silicates typically carry a negative charge, while oxides, carbonates, and hydroxides are predominantly positive across a broad pH range (Kosmulski, 2009). DNA, particularly its phosphate backbone, which is negatively charged above a pH of 5, has been observed to primarily interact through this component (Vuillemin et al., 2017; Yu et al., 2013). This backbone can engage directly with positively charged surfaces due to electrostatic forces. However, the presence of polyvalent cations is a determining factor when it binds to a negatively charged surface (Feuillie et al., 2015; Greaves & Wilson, 1969; Lu et al., 2010; Maity et al., 2015; Michalkova et al., 2011; Nguyen & Chen, 2007; Saeki et al., 2010). A high charge density on mineral surfaces can lead to the adsorption of closely bound water molecule layers (Geissbühler et al., 2004; Lee et al., 2010). Such layers have been theorized to enhance DNA hydrolysis (Ye et al., 2011). The DNA molecule can adsorb to the mineral via water layers or penetrate the water layers and interact with the mineral directly, where the latter is expected to form a stronger bond than the former. The consistency of water layers cannot be predicted from a bulk measure of surface charge. Instead, the structure of the water layer is dependent on local topography and local charge distributions on a mineral surface. Generally, it's difficult for molecules to navigate through tightly bound surface water layers (Cooke et al., 2010; Sparks et al., 2015; Yang et al., 2008; Zhu et al., 2013). Surface irregularities, such as steps or defect sites, are vital since they disrupt the water's structure, creating a more receptive binding site (Aschauer et al., 2010; Cooke et al., 2010; Freeman et al., 2012; Sand et al., 2010; Spagnoli et al., 2006). Similarly,

naturally occurring features like step edges or etch pits on a mineral surface present varied charge interactions compared to the flatter areas, leading to different adsorption affinities (De Yoreo & Vekilov, 2003).

Many studies that explore DNA adsorption to mineral surfaces typically employ bulk methods, relying on bulk values such as surface charge, adsorption capacity, and active sites. However, our mechanistic understanding of DNA–mineral associations remains limited. Specifically, we are yet to fully understand which mineral surface group the DNA molecule bonds to across a surface, how strongly the DNA is bonded, which sites at the surface the DNA bonds to, and how the local adsorption behavior and subsequent preservation are influenced by solution chemistry? According to interfacial geochemical principles, the answer to those questions varies with mineral characteristics and the solution chemistry. By acquiring a deeper, mechanistic comprehension of the interplay between mineralogy, DNA, and solution composition, we stand a much better chance of understanding the processes driving eDNA taphonomy. Additionally, we can assess whether variations in mineralogy across different environments impact the DNA preserved in eDNA reservoirs. Beyond this, grasping DNA–mineral interactions at a foundational level might also open avenues for leveraging sediment provenance data to enrich our interpretations of retrieved DNA. Obtaining mechanistic information is inherently challenging, and in the case of eDNA taphonomy, the many parameters and variables involved in DNA taphonomy essentially comprise a little explored research field. Here we study the DNA adsorption dynamics and mechanisms in two distinct mineralogical systems as a function of solution composition. We use two novel approaches: Atomic force microscopy (AFM) and molecular dynamics (MD) simulations, and focus on the basal planes of mica and the (10.4) surface of calcite.

Mica is a clay mineral with atomically flat, uniform, and negatively charged basal planes and positively charged edge sites. This mineral essentially serves as a representative model for most clay basal planes that terminate with silica tetrahedrons. Bulk DNA adsorption to a wide range of clay minerals has been widely studied, and a few studies have studied DNA adsorption to mica using AFM (Murugesapillai et al., 2017; Pastré et al., 2006). In this study, we focus on the basal plane (we elaborate on the consequences of the edge sites in the discussion), where, because of the negative charge, the DNA is expected to need charge-dense cations to facilitate a bridge between the negatively charged DNA backbone and the clay basal surface. Calcite, in contrast to mica, remains predominantly positively charged under most environmental conditions and features a diverse distribution of charges and topography. The (10.4) face, which is both commonly expressed and energetically stable in natural calcite, consists of atomically flat terraces intersected by step edges (Figure 1d). Calcite's unique orthorhombic and rhombohedral structures result in two distinct step edges: obtuse and acute. These edges can be terminated either by carbonate or calcium ions, bestowing locally positive or negative charges toward the solution. Overall, the mica basal plane represents the adsorption behavior of silicates in general, and calcite conceptually represents positively

FIGURE 1 Atomic force microscopy images of mica showing the conformation of adsorbed plasmid DNA with different background ions. The DNA is visible as white (highest points in the image) lines. (a) Mica-DNA in NaCl; (b) Mica-DNA in $MgCl_2$; and (c) Mica-DNA in $NiCl_2$. (d) Calcite only. Freshly cleaved and after 2 min. Exposure to the buffer solution used when adding the DNA to the surfaces. The image shows step edges on steps and etch pits. (e) Calcite-DNA in buffer. The surface displays etch pits and adsorbed DNA. The etch pit morphology is determined by the underlying orthorhombic structure of the calcite crystal, which is oriented such that the obtuse corners are oriented south-west and the acute corner is oriented toward north-east. (f) Calcite-DNA in NaCl. (g) Calcite-DNA in $MgCl_2$. (h) Calcite-DNA in $NiCl_2$. (i) Adsorbed plasmid DNA on a Poly-L-lysine substrate. The DNA is supercoiled and was deposited with 10 mM NaCl as a background electrolyte.



charged mineral surfaces and illustrates how topography, charge density, and water layer disruption can change the adsorption affinity of biomolecules. Calcite is directly relevant for eDNA studies from carbonates (e.g., speleothems (Baker et al., 1996; Brennan & White, 2013; Dhami et al., 2018; Mendoza et al., 2016; Stahlschmidt et al., 2019) and corals (Selkoe et al., 1829)) and can be used as a guide for expected DNA-mineral behavior for oxides as well.

In this study, we utilize mica and calcite surfaces to emphasize the diverse effects mineral surfaces can have on eDNA taphonomy and their relationship with solution chemistry. We further discuss the implications of retained and preserved eDNA and underscore that the accuracy of stored biodiversity estimates is contingent upon an understanding of mineralogy, environmental chemistry, and dominant taphonomic processes. Our approach employs Atomic Force Microscopy (AFM) to scrutinize DNA adsorption behavior and binding affinity to both calcite and mica surfaces in the presence of three environmentally relevant ions (Na^+ , Ca^{2+} and Mg^{2+}) with distinct ionic potentials (charge/radii). The different solution chemistries are chosen to illustrate the importance of the depositional environment for the retention of eDNA in sediments. For our study, we used plasmid DNA, which precludes interaction from the base pairs in an open strand, ensuring compatibility with our modeling approach that begins with a closed strand configuration. We generated etch pits on the calcite surface to increase the amount of step edges on the calcite crystals during adsorption to understand if there was a preference of DNA for adsorbing to terrace or edge sites, and acute or obtuse steps. We used chemical force microscopy to establish if

solution composition and mineralogy would change the strength of the DNA-mineral binding affinity subsequently. Results from our MD simulations support the observed binding preferences as seen with the AFM and help to understand the reason for them. Finally, we used in-situ AFM imaging to monitor the adsorption behavior of the adsorbed DNA.

2 | MATERIALS AND METHODS

2.1 | Minerals

Single crystals of optical quality Iceland spar calcite (purchased from Ward's Natural Science). The mica were grade V1, had a diameter of 1 cm and were purchased from Ted Pella Inc.

2.2 | Chemicals

The salts ($NaCl$, $MgCl_2$, and $NiCl_2$) were reagent grade and purchased from Sigma-Aldrich, and used without purification. The Poly-L-Lysine was purchased from Boster Biological Technology and used as received. The DNA was the double-stranded plasmid: pUC19. It is composed of 2686 base pairs and is approximately 910 nm long. The plasmid was purchased from Integrated DNA Technologies IDT. For imaging and sample preparation, we used a nuclease-free Tris buffer at pH 7.5 purchased from Sigma Aldrich. All solutions were prepared

using ultrapure water from a MilliQ deionizing column (resistivity >18 M Ω cm; Millipore Corporation). The artificial seawater solution was prepared following the protocol by Kester et al. (1967).

2.3 | Substrate preparation

Calcite samples were cleaved in air, and the calcite dust was immediately removed with a firm stream of N₂(g). The mica was cleaved with a piece of tape. The Poly-L-Lysine film was prepared on freshly cleaved mica by using a 10 μ L droplet of Poly-L-Lysine at a concentration of 0.01 w/v in MilliQ water. After 30 s, the surface was rinsed with plenty of MilliQ and blow dried with N₂(g).

2.4 | Preparation of DNA on the minerals

A 10 μ L droplet of plasmid DNA pUC19 at a concentration of 0.4 ng/ μ L and 10 mM electrolyte was placed on a freshly cleaved mica or calcite. The droplet was left for 2 min before being rinsed with 400 μ L of MilliQ. The mineral was dried with a soft blow of N₂(g) for 30 s.

2.5 | AFM imaging

For scanning in air and liquids, we used a Cypher and a Cypher VRS from Oxford Instruments. Both were running in tapping mode. For the imaging in air, we used aluminum-coated AC240TS silicon tips from Olympus with spring constants between 0.6 and 3.5 N/m and a resonance frequency approximating 70 kHz. For tapping in liquid, we used BL-AC10DS from Asylum Research, Oxford Instruments. We used a spring constant of 107 pN/nm and a resonance frequency of 1500 kHz. The spring constants were determined using the Sader method (Sader et al., 2012). For both instruments, the force between the tip and the sample was varied to minimize the force exerted by the tip on the surface. Scan angle, scan rate, and set point were systematically varied. We measured multiple sites on every sample, and the experiments were repeated several times. For the fragmentation experiments, we prepared the sample as for the experiments performed in air and imaged the surface in air to confirm that we had intact plasmids. Subsequently, we introduced the calcite-saturated buffer to the surface and began the approach process.

2.6 | Chemical force microscopy (CFM)—surface chemical analysis

After the tips were checked under a microscope, they were cleaned with water for molecular biology, ethanol, and finally ultraviolet ozone cleaner for 20 min. Subsequently, the tips were functionalized overnight with a self-assembled monolayer (SAM) solution terminating in a phosphate (PO₄³⁻) end group (Sigma-Aldrich, 754269). Then, the tips were washed in ethanol (3 \times), and allowed to dry on glass

slides in a petri dish at room temperature. Like AFM imaging, we used a Cypher and a Cypher VRS from Oxford Instruments and BL-AC10DS from Asylum Research from Oxford Instruments for tapping in liquid. For these measurements, we used OBL-10 silicon nitride tips from Bruker with spring constants between 0.03 and 0.009 N/m and a resonance frequency approximating 70 kHz. A constant trigger force of 80 pN was used, and the spring constants of the levers were determined by thermal noise method (Butt & Jaschke, 1995; Hutter & Bechhoefer, 1993). We recorded force-distance cycles at a 3 μ m scan size, 300 nm force distance, and 1 Hz scan rate, and both approach and retract velocities are approximating 1 μ m/s. For the CFM force map, force lines and points are constant at 14 N, and the scan angle is zero degree. We performed the measurements in liquid at concentrations of 10 mM (NaCl and MgCl₂) and 100 mM (NaCl and MgCl₂), pH 7. For each solution parameter, the experiment was repeated several times, and the average was calculated. A single tip of each type was used for tapping mode on the surfaces of freshly cleaved mica and calcite to ensure that the spring constant and tip radius were constant. At least we carried out two independent measurements to check the uniformity of our analysis.

2.7 | MD simulations

All molecular dynamics simulations were performed using DL_POLY classic (Smith & Forester, 1996). Simulations were carried out in the NVT ensemble with a temperature of 300 K and a thermostat relaxation time of 0.1 ps. The leapfrog verlet algorithm was used with a timestep of 0.5 fs. Coulombic interactions were modeled with the Ewald method (precision 1×10^{-6}). Periodic boundary conditions were used for all the simulations.

The calcite forcefield was taken from (Raiteri & Gale, 2010) using SPC/E water. The DNA forcefield was taken from the AMBER forcefield (Cornell et al., 1995). Water-DNA interactions were calculated using the standard Lorentz-Berthelot mixing rules. The Ca-N interactions were taken from Freeman et al. (2009), Ca-O (in DNA) were fitted using the Schröder method as described in (Freeman et al., 2007). The terms are listed in the supplementary material.

The DNA molecule was a random double helix with the sequence C(G)-A(T)-A(T)-G(C)-T(A)-T(A)-T(A)-A(A)-G(C)-C(G)-T(A)-, where A is adenine, T is Thymine, G is guanine, and C is cytosine. The complementary base is listed in brackets. The periodic simulation cell was constructed such that the z cell parameter size matched the chain length of the 11 base pair chain (39.5 Å). This meant the DNA chain periodically spanned the boundary conditions (i.e., the end C(G) connected with the other end T(A)). The calcite slab was built in Metadise (Watson et al., 1996) from a geometry optimized cell in GULP (Gale, 1997). The slab was cut to express the (10.4) surface of calcite. Steps were added by removing Ca and CO₃ ions from one surface and placing them on the other surface in the appropriate lattice positions. After all surface cuts and reorganizations the calcite slab was relaxed in vacuum. The final cells consisted of 8 CaCO₃ layers with 768 formula units with surface vectors 47.8 Å \times 39.5 Å.

For the adsorption studies, the DNA was placed parallel to the surface with the center of mass $\sim 11 \text{ \AA}$ from the calcite surface. One thousand two hundred and sixty-eight water molecules and 11 Ca^{2+} cations (so-called free Ca for charge compensation of the negatively charged DNA) were then randomly placed $\sim 6 \text{ \AA}$ from the surface using the Packmol package (Gale, 1997). By placing the water molecules further from the surface, this ensured the DNA was able to initially interact with the surface and not be automatically displaced by the smaller and more mobile water molecules and cations. Perpendicular to the surface, a large vacuum gap of $\sim 60 \text{ \AA}$ separated the DNA/water from the unsolvated Ca surface. Across this gap, a repulsive barrier was added to ensure water molecules were unable to desolvate from one calcite surface and move to the vacuum surface.

2.8 | DNA fragmentation in bulk experiments

2.8.1 | DNA adsorption

Two hundred microliters of elution buffer EB (Qiagen) were added to 20 mg of calcite powder (Sigma) and after sonication for 15 min. One μg of 1000 bp DNA fragment (Thermo Scientific™) was added in 300 μL EB buffer to the calcite samples (C1, C2, and C3). The samples and two negative controls containing only calcite powder with no added DNA (samples 5 and 6) were incubated on a rotor for 4 h. To mimic the AFM experiments, we added 250 μL of molecular biology-grade water (BioNordika) to disequilibrate the system, allowing for slight DNA desorption and re-adsorption. After 1 h of equilibration, we added another 250 μL of water and incubated them overnight. The samples were centrifuged for 1 min at 13,000g, and the supernatant was extracted and used to measure the equilibrium concentration on a Qubit dsDNA High-Sensitivity assay (HS; Thermo Fisher Scientific). None of the extracted supernatants had measurable DNA. Finally, we washed the samples with 1 mL of EB buffer and centrifuged the samples for 1 min at 13,000g. We retained the supernatant and measured the DNA concentration of the wash solution on Qubit. Only the wash solution from sample C2 had a measurable amount of DNA, which was 0.0134 ng/ μL (13.4 ng total).

2.8.2 | DNA extraction

After adsorption, samples were incubated overnight in 1 mL of 0.5 M, pH8 EDTA buffer (Invitrogen™) to release the DNA bound to calcite. In this step, we added a positive control (samples 6, 7) where one μg 1000 bp DNA fragment was added to 1 mL of EDTA and incubated overnight. All calcite-DNA samples (Giguet-Covex et al., 2019; Haile et al., 2007; Hofreiter et al., 2003) and negative controls (just calcite; Pedersen et al., 2016; Slon et al., 2017) dissolved in EDTA during the incubation time. To purify the released DNA from EDTA, we desalted the samples using 10 kDa Amicon® Ultra-4 Centrifugal Filter Unit (Millipore). We used a centrifuge with a swinging-bucket

rotor at 4000g for ~ 35 min until $\sim 100 \mu\text{L}$ were left. Then we added 3 mL of molecular biology-grade water and centrifuged the samples until $\sim 100 \mu\text{L}$ were left. We repeated this step twice. Afterward, we measured the DNA concentration on the Qubit dsDNA Broad-Range assay (HS; Thermo Fisher Scientific) and sent the samples for the fragment analysis on Fragment Analyzer (5300; Agilent) at the GeoGenetics sequencing core, University of Copenhagen.

3 | RESULTS

3.1 | DNA adsorption behavior as a function of solution composition

We applied the same experimental procedure to both mica (negatively charged) and calcite (positively charged) surfaces to compare the DNA conformation and adsorption behavior between the two types of surfaces using AFM. We applied three different 10 mM solutions of NaCl, MgCl_2 , and NiCl_2 , leading to two different ionic strengths: 10, 30, and 30 mM, and three distinct ionic potentials: 1, 12.5, and 16, respectively. Adsorbing the DNA on the negatively charged mica was, as expected, sensitive to cationic composition. When NaCl was used as the background electrolyte, the DNA, seen as thin white lines on the surface, did not adsorb to the mica surface (Figure 1a). With MgCl_2 , the full plasmid is adsorbed, and generally in a ring form or with one or two coils (Figure 1b). When NiCl_2 was used, the DNA adsorbed as supercoils and the circular rings were not observed (Figure 1c), indicating the stronger adsorption is preventing relaxation of the structure. Our results on DNA adsorption on mica agree with previously reported data (Zhai et al., 2019). Calcite is slightly water soluble and during the adsorption process, the DNA was added to calcite using a solution undersaturated with respect to calcite. This procedure causes a slight dissolution of the calcite surface resulting in the formation of etch pits (Figure 1d). The occurrence of edge sites surrounding the etch pits enabled us to assess if the DNA prefers such sites or accompanying terraces. The DNA adsorbs predominantly at the step edges, with a clear preference for the acute step edges (Figure 1e). A part of the plasmid ring reaches across terraces to bridge adjacent steps in order to maximize the plasmid's interaction with step edges. The adsorption behavior highlights that the interaction between DNA and the step edges is more favorable than between the terrace sites. A plasmid that showed preference toward adsorption on a terrace was not observed. No electrolytes were added to the experiment, but in contrast to the solutions used in the mica study above (Figure 1a–c), there is always calcium present in the calcite system as calcite is a sparingly soluble salt and its surface will dissolve in calcite-undersaturated solutions. Although the resulting calcium concentration is much less than the 10 mM used for the background electrolyte, we cannot, from Figure 1e, rule out any effects that calcium ions in the solution have on DNA adsorption.

Applying the same range of background electrolytes as for mica (Figure 1f,g), we do see plasmid adsorption to calcite with the NaCl

electrolyte (Figure 1f). We were not, however, able to discern any differences in DNA adsorption to calcite with either the added NaCl or MgCl₂ background electrolytes (Figure 1f,g). In the experiments where NiCl₂ was used, we observed twisting of the helix (Figure 1h) but the plasmid was still confined to the step edges and hence, probably did not have the freedom to coil as seen on the mica surface. Similar to Figure 1e, we observed no adsorption where the majority of the DNA was bound to the terraces. This indicates that the steps, and hence the mineral surface charge density, is the determining factor controlling DNA adsorption to calcite and that the ionic potential of cations does not play as important a role as seen for DNA adsorption to mica.

Surface charge density plays an important role in the behavior of electrolytes and polymers near surfaces (Israelachvili, 2011; Jelavić et al., 2018). As highlighted in Figure 1a–c,f,g, the ionic potential of the background ion plays a large role for the adsorbed conformation of the DNA on the negatively charged surface and much less so for the positively charged surface. For mica the higher the charge density the more supercoiling, for calcite an effect was only seen for Ni, both systems indicate that the charge densities available at the surface play a role for how much the DNA coils during adsorption. To test if the high surface charge density would lead to supercoiling (Figure 1i), we fixed a positively, densely charged polymer (poly-L-Lysine) on a flat mica substrate. According to our predictions, the DNA supercoiled without the presence of charge dense background cations.

3.2 | Role of solution composition on DNA-mineral interaction strength

Although AFM images offer a visual representation, they do not reveal whether the strength of DNA-mineral interactions is influenced by distinct ions or whether DNA inherently binds more robustly to calcite compared to mica. To investigate this, we used chemical force microscopy (CFM) to probe the dependence between the overall surface charge, the ionic potential of cations, and the ionic strength of the solution. Utilizing both phosphate and amine-terminated AFM tips representing the interaction between the phosphate backbone and the basepairs, we quantified the adhesion forces between calcite and mica surfaces, as illustrated in Figure 2. The adhesion forces between the phosphate group and the calcite surface were, in general, higher than the forces between the phosphate tip and the mica surface. Across the applied sequence of solutions (10 mM NaCl, 100 mM NaCl, 10 mM MgCl₂, 100 mM MgCl₂, and 10 mM NaCl) both minerals had the strongest interaction with 100 mM MgCl₂, i.e., with a high concentration and a high ionic strength. The phosphate–mineral adhesion strength, however, showed different relative dependencies between the specific solutions. For mica, the adhesion forces were largest when adding 10 mM Mg and far larger than 100 mM NaCl, indicating that at lower ionic strengths, charge density at the surface is more important than

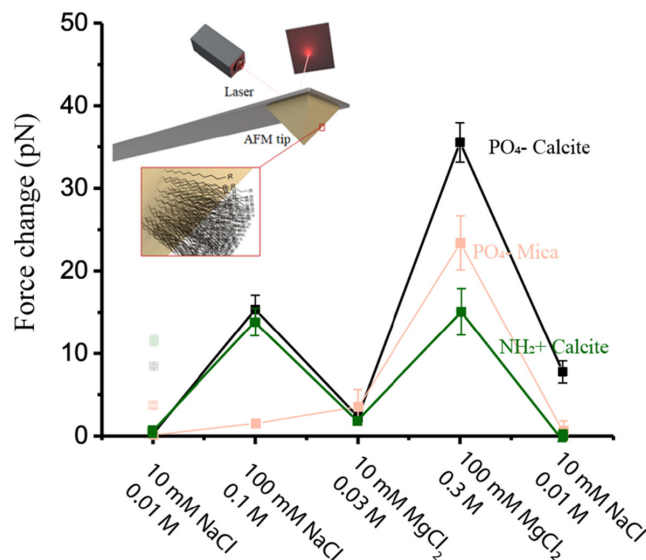


FIGURE 2 Adhesion force between a phosphate and an amine terminated AFM probe and a calcite and a mica surface in a sequence of different concentrations of NaCl and MgCl₂ solutions. The corresponding ionic strength is stated under the concentrations of each solution. The first measured point is placed at 0 pN for easier comparison of the force changes. The transparent points at 10 mM NaCl show the force measured. Insert show the AFM tip and the functionalization where R represent the phosphate or amine functional group. Insert modified from Jelavić et al. (2020).

high salinity and the screening of the surface charge. For calcite, the adhesion strength was highest in the two high-concentration solutions, indicating that the thickness of the electrical double layer has a dominating role in DNA binding. Interestingly, examining calcite forces for 10 mM reveals that the surface retains a “historical” imprint of prior solutions. This is evident from the augmented adhesion force for the 10 mM NaCl observed post the 100 mM MgCl₂ solution, suggesting an incomplete exchange of Mg ions with Na ions. It should be highlighted that this “memory” was not observed with mica, given it was re-cleaved before each force measurement, eliminating the possibility of retaining pre-adsorbed Mg ions. Finally, it is worth noting that the adhesion forces measured for calcite represent an average over both the steps and terraces. In general, the force distribution for calcite was broader than for mica, which is expected as the calcite surface contains binding sites (steps and terraces) with different affinities for binding. For the amine functionalized tip, we, similar to the case of phosphate and calcite, saw a strong dependence on adhesion strength with ionic strength.

3.3 | Mechanism of DNA-calcite interaction using MD simulations

MD simulations provide a detailed view of how the DNA molecule orientates itself relative to a mineral surface, the binding stability

and the type and numbers of bonds involved. The DNA molecules show distinct behavior between the flat terraces (10.4) and the step edges.

3.3.1 | Terraces

At the beginning of the simulations of DNA with the terrace (10.4 surface labeled configurations 1–6), the separation between the center of mass of the DNA (i.e., the approximate center of the cylindrical DNA) and the calcite surface is $\sim 11\text{Å}$. Given the radius of the DNA cylinder is $\sim 9\text{Å}$, this relates to parts of the DNA molecule being in close or direct contact with the surface. As the simulations progress, the DNA moves perpendicularly away from the surface by an average of 1.96Å as evidenced by the change in the center of mass to surface separation (Figure 3a). The final distance between the surface and the center of the DNA molecule shows that the DNA moved above the tightly bound water layer on the calcite surface. The change in distance leaves a few direct interactions between the DNA and the calcite surface. Table 1 lists the direct interactions between the calcite surface and DNA molecule during the simulation and in only three of the six configurations, the DNA is able to penetrate the water layer and make direct interactions with the (10.4) surface. In two such cases (configurations 2 and 5), oxygen atoms from the phosphate groups bind to calcium cations on the surface, and in one case (configuration 3), part of the adenine base interacts with the carbonates on the surface. Examples of these interactions (for other cases) can be seen in Figure 3b,c and the interactions are generally present throughout the simulation, implying they are stable. Configurations 2 and 5 show the least perpendicular movement away from the surface.

There are a total of 26 unique H-bonds normally present between the two strands in the double helix. Over the course of the simulation, those H-bonds will break and reform due to structural fluctuations related to normal thermal motion. When the DNA is

run in a neutralized waterbox with no surface present, an average of 21.8 H-bonds (with a standard deviation of 1.95) are present at any one time in the simulation. When placed in contact with the surface, we generally see small changes in the number of H-bonds, and the DNA structure is largely unaffected by the surface (see Table 1). The changes are small shifts in the lifetime of the H-bonds (full details are found in the supporting Information), giving an overall reduction in the number of H-bonds.

The structure of the two chains still resembles the entwined double helix, and the disruption is considered minor. Only in configuration 3 are more significant changes observed. In this configuration, an adenine base comes out of the backbone and H-bonds to a carbonate group on the calcite surface. The loss of the base from the chain does not lead to a complete breakdown of the DNA structure but does significantly disrupt three of the base interactions (2 between cytosine number 10-guanine number 2 and 1 between thymine 11-adenine1), which leads to a net loss of ~ 3 H-bonds (Table 1, configuration 3). The net loss is within 2 SD of the mean, and hence could be described as a small disruption to the structure.

The charge-neutralizing calcium that is free in the solution does not get involved in the binding process, and none of them form interactions with the DNA (Table 1). Direct interactions between free calcium cations and oxygen atoms in the DNA molecule would break up the tightly bound solvation shells around the cations and are therefore unlikely to be energetically favorable. This suggests that the free ions are not key to the binding, which agrees with our AFM experiments, as the choice of electrolyte did not dictate whether binding occurred or not. The general, infrequent interactions between the free Ca and the DNA agree with our AFM where we observed little evidence of clumping or aggregation of the DNA molecules, which are normally reported in liquids with divalent cations (Duguid & Bloomfield, 1995).

Between the six different helix configurations at the flat terraces, the average energies vary by only 75kJ/mol , and we do not find any correlation with the number of interactions with the

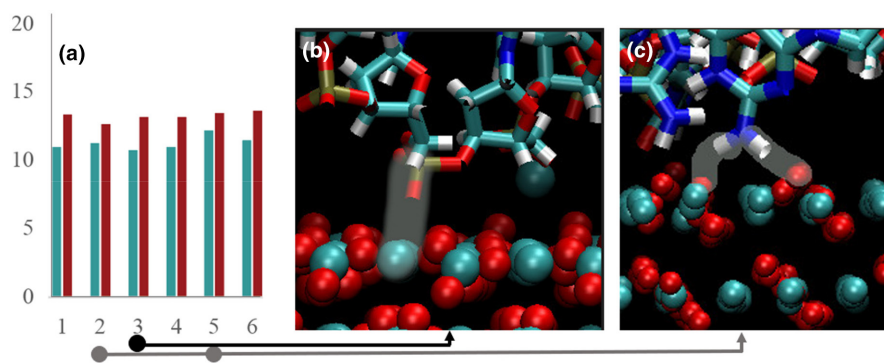


FIGURE 3 DNA-surface separation and example images of the direct interactions between the calcite surface and the DNA molecule. The interactions are highlighted to make them more visible. (a) Separation perpendicular to the surface between the center of mass of the DNA molecule and the calcite surface. Initial position (green) vs final position (red). DNA has a radius of 9Å . (b). showing an example interaction of the O of the phosphate group and the Ca of the calcite as seen in configurations 2 and 5. (c) Showing an example of the H of a NH_2 group with O of the carbonate as seen in configuration 3. Key: O (red), H (white), C (cyan), Ca (cyan), N (blue), and P (gold). Figure (b) taken from obtuse calcium step (configuration 7) and (c) taken from acute calcium step (configuration 17) acute step.

TABLE 1 Change in H-bonding between residues in the two separate helices (from an average total of 21.8 ± 1.95) and list of the number of interactions between surface calcium with O in DNA, DNA $\text{NH}_2\text{-O}(\text{carbonate})$ in the surface and solvated calcium with O in DNA.

Terrace (10.4)	H-bonds change	Surface Ca-O	$\text{NH}_2\text{-O}(\text{carbonate})$	Free Ca-O
1	-1.6	0.0	0.0	0.0
2	+0.7	5.0	0.0	0.0
3	-2.9	0.0	1.6	0.0
4	-0.1	0.0	0.0	0.0
5	+0.5	1.0	0.0	0.0
6	-0.3	0.0	0.0	0.0
Acute carbonate + obtuse calcium				
7	-3.1	3.0	0.0	0.0
8	-1.9	0.0	0.0	0.0
9	-5.9	1.8	0.0	0.0
10	-3.5	0.0	0.0	0.99
11	-4.8	0.0	0.0	0.91
12	-0.7	0.0	0.0	0.0
Acute calcium + obtuse carbonate				
13	-1.8	0.0	0.0	0.0
14	-9.4	0.0	4.2	0.0
15	-13.6	0.0	2.0	0.0
16	-6.1	0.8	4.1	0.0
17	-10.9	1.0	4.0	0.0
18	-1.8	0.0	0.0	0.0

Note: Averages calculated over the last 500ps of simulation. An interaction between DNA and surface or ions is defined as a maximum separation of 3 Å. An H-bond is defined as occurring between H and either an N or O atom at maximum separation of 2.1 Å.

surface. Configuration 3 displays the highest energy and is where the adenine base has twisted out of the helix, suggesting that the energy gain associated with the surface binding does not outweigh the energy loss from the structural changes in the DNA molecule.

3.3.2 | (10.4) steps

The step structures used are shown in Figure S2. As observed in the AFM images, the stepped surfaces show different adsorption behavior than the terrace. The DNA strand started parallel to the edge of the periodic steps, enabling us to measure the separation parallel to the surface from the center of the DNA chain to the calcium-and carbonate-exposed step edges. At both surfaces we see a tendency for the DNA molecule to move toward the calcium-exposed step (Figure 4a). Due to the geometry of the calcite, the calcium-exposed step edges have a block of positive charge, which attracts the negatively charged DNA backbone. The migration observed in the simulations demonstrates that the DNA will diffuse across the flat terraces and stop at the step edges. Examining Figure 4a, we

can also notice that the DNA generally ends far closer to the acute calcium step edge than to the obtuse step edge. Both of these observations are in agreement with our experimental results in Figure 1e showing the DNA molecules adsorb at the step edges with a preference to the acute sites.

As also observed for the (10.4) terrace, the bulk of the DNA strand resides above the organized water layers on the step surfaces. In half of the step-based simulations, there are no direct interactions between the DNA and the calcite surface. On the acute carbonate step surface, we observe two cases of the phosphate O backbone interacting with the Ca in the surface (configurations 7 and 9). On the acute calcium step, we also see two cases of the backbone O phosphate with the surface (configurations 16 and 17). The remaining four direct interactions (configurations 14–17) come from the DNA bases that fold out of the helix on the acute calcium+obtuse carbonate step (Table 2). Of the bases that fold out of the DNA the same cytosine base is observed in all cases and the same adenine base is observed in three of the four cases suggesting that these are a particularly vulnerable part of the DNA sequence to folding out of the chain and binding. Two guanine bases are observed to interact directly with the surface in configuration 17. We never observe any thymine bases in contact with the surface which may be due to the random sequence and particular structure rather than their lack of NH_2 amine groups. The NH_2 group appears to be the major driver to the binding in the cases where the bases interact with the surfaces (Table 1) and remain relatively stable throughout the simulation.

The free calcium ions in the solution do not generally interact with the DNA (Table 1) but frequently cluster around the carbonate-terminated step due to the block of negative charge there (from the carbonate anions). In the simulation, we observe two cases where the DNA does interact with the free Ca in solution (configurations 10 and 11). In these cases, there is one loose Ca in the solution that interacts with the phosphate O. The interaction with the Ca ions does not operate as a bridge to the surface or similar feature.

Compared to binding at the (10.4) terrace, the DNA undergoes a more significant structural change at the step edge. Even though only half of the configurations are binding to the surface directly, we see a significant loss of H-bonding in most of the configurations at the steps, suggesting a general loss of inter-helix H-bonding rather than simple redistributions. This average loss of H-bonds is far larger at the steps (-0.62 on the (10.4) terrace, -3.32 at the acute carbonate, and -7.27 at the acute calcium) and beyond a single standard deviation from the mean. Visual inspection shows a significant change in the DNA structure in some of the most affected configurations. From snapshots of the simulation progress, we can identify particular cases of the breakup and obtain a better understanding of the process. Figure 4b shows a snapshot of configuration 7, where several backbone phosphate O interact with the surface, but there are no surface interactions from the bases. We have highlighted the double helix structure to show how the helix is largely retained during the simulation despite an average loss of 3.1 H-bonds, which can be partially observed in the twisting of two bases within the helix (see the area highlighted with the arrow). Figure 4c shows configuration 17 with a top-down view (effectively

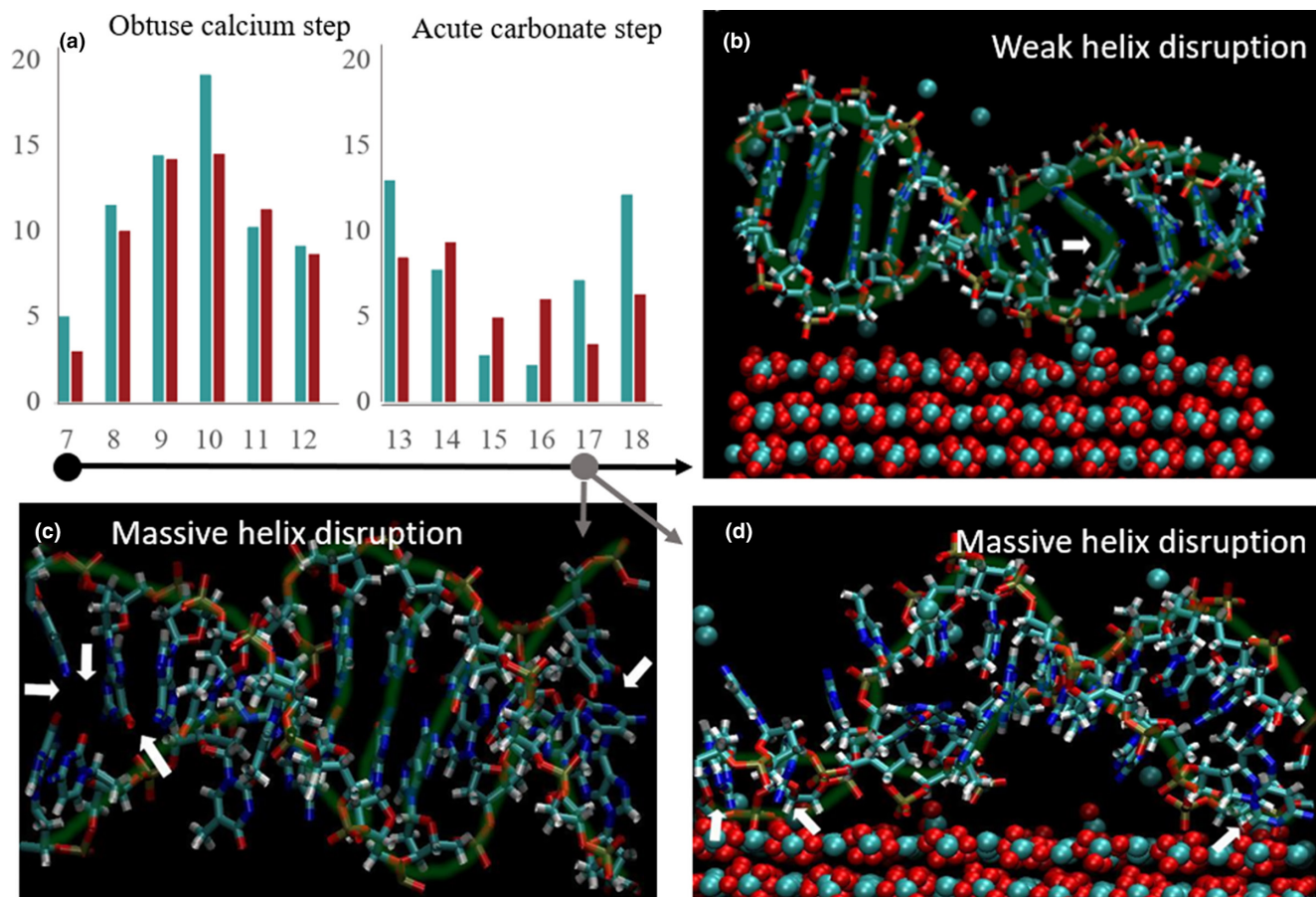


FIGURE 4 (a) Separation parallel to the surface of the center of the DNA molecule to the Ca-exposed step. Bars show starting separation (green) and final separation (red). Configurations 7–12 are the obtuse calcium step surface. Configurations 13–18 are the acute calcium step. (b) DNA on the acute carbonate surface in configuration 7. The double helix structure has been highlighted in green to aid the eye. (c and d) DNA on the acute calcium step edge in configuration 17 shows the break out of the bases. The double helix structure has been highlighted in green to aid the eye. (c) show the top view looking down onto the surface (calcite surface not shown for clarity) and (d) the side view. Arrows are added to images to highlight the breakdown of DNA structure in (c) and where bases bind to surfaces in (d). Key: O (red), N (dark blue), Ca (cyan), P (gold), C (cyan), H (white), water not shown for clarity.

TABLE 2 Listing the specific DNA bases that directly interact with the calcite surface for the acute calcium step system.

Configuration	Bases
14	Cytosine a1, adenine a3
15	Cytosine a1, adenine a3
16	Cytosine a1, adenine a3
17	Cytosine a1, guanine a9, guanine b2

Note: Bases are labeled with “a” for one helix and “b” for the other helix.

looking at the plane of the calcite surface), it can be seen that one of the helix folds (the left and right-hand ends of the image) has effectively opened and the bases moved apart (indicated by the arrows in Figure 4c). The side view in Figure 4d shows how several residues move out of the core of the DNA molecule to bind to the acute calcium-exposed step causing a major structural breakdown of the DNA (highlighted with the white arrows in Figure 4d). We can also see that several bases are free but not interacting with the surface (left-hand end of the image). Only in the central area of the DNA chain that can be

seen more clearly in Figure 4c is the helix preserved. In configuration 17 the DNA only has an average of 10.9 H-bonds left between its two helices, from the original 21.8 H-bonds. The results suggest that there is a strong attraction for the molecule at the step that is best achieved with the structural deterioration of the DNA molecule. The relatively low conformational freedom of the DNA molecule due to the periodic boundary conditions in the simulation likely prevents the full breakdown of the chain, which may occur in a real system.

The large positive charge at the calcium step edges will create a driving force to pull the DNA across the terraces toward the steps. It is likely that this positive charge build up may cause deformations in the negatively charged phosphate backbone. The loss of H-bonds is larger at the step edges than on the terraces, even when we see no evidence of the bases moving out of the helix (e.g., configuration 9 at the step). Once a base pair is separated from its opposite base pair, then it is free to twist out of the chain and interact with the surface, where it can make favorable interactions with both the step surface and terrace. The interactions between the DNA and the surface are most significant at the acute-calcium step edge. The acute step edge has previously

been shown to have a more broken water structure compared to the obtuse step (Dhami et al., 2018; Mendoza et al., 2016) meaning that the binding of molecules is easier since there is less tightly bound water to displace. Binding of negative functional groups has also been highlighted in other molecular dynamics simulations.

In most cases, the DNA was observed to move toward and interact with the calcium-exposed step edges while avoiding the negatively charged carbonate-exposed step edges. At the end of the simulation, some of the free calcium is often found in the vicinity of the carbonate-exposed step edge, as would be expected due to electrostatic interactions between the two. We further explored if calcium ions associated with a carbonate step edge would facilitate DNA binding. We made a set of starting configurations with all the free calcium within approximately 6 Å of the acute carbonate exposed edge. In this situation, we observed that the DNA began ~13 Å from the calcium-exposed carbonate step and did not move any closer to the acute-calcium step and instead remained close to the carbonate edge with the exposed calcium ions. This highlights that the presence of solvated calcium around the edge can neutralize the negative charge around the step and create a positive field that attracts the DNA molecule and therefore both acute step edges may favorably bind the DNA. It is difficult to isolate this interaction in the AFM experiments because we cannot know which step edges are terminated with carbonate versus calcium. There will be free calcium ions in the solution due to the dissolution of the calcite surface, which could interact with the carbonate-terminated step edge, so this is a possibility in the real system. We should stress that we cannot observe ion structuring around the steps in the AFM experiments and we only explored 1 pH value in the experiments, which will affect the step structure and ion concentrations. In the AFM experiments, however, we see DNA binding to the majority of the steps.

Comparing the energetics of DNA binding across the systems is not trivial due to the changes in DNA conformation during the simulation and the free ions in solution. Figure S3 shows the energy of each configuration with respect to the lowest energy configuration for that surface type (e.g., only comparing acute calcium and obtuse carbonate to other configurations with acute calcium and obtuse carbonate) against the number of H-bonds present between the DNA helices. We can see a general trend is that as H-bonds are lost from the DNA, the energy of the total system increases. This implies that those systems with more direct DNA-surface interactions will be higher in energy as the DNA loses its structural integrity. The significant changes in the DNA structure between the configurations also mean that it is not possible to do a direct comparison of the adsorption energy between different surfaces as the DNA in the reference system is in a very different configuration (i.e., a perfect DNA molecule).

3.4 | Dynamics of the adsorbed DNA on calcite

3.4.1 | In-situ dynamics and fragmentation

The MD simulations are made in liquid, and to ensure compatibility between the MD simulation and AFM images we made in air, we

used fast scan the AFM to observe the dynamics of the adsorbed DNA to calcite. The dynamic mode revealed that the DNA molecules were fragmenting, as predicted by the MD simulations. After the initial adsorption of the DNA, we slightly disrupted the equilibrium to induce dissolution of the calcite steps to initiate a desorption and re-adsorption process, forcing the DNA molecules to relocate to allow us to visualize any fragmentation as a result of binding. The fragmentation is evident in Figure 5, which shows a time-resolved sequence of the same area displaying ongoing dissolution of the surface and DNA desorption and re-adsorption. The arrow in Figure 5a points to a DNA-free section of a step edge. In Figure 5b, the space is filled, the terrace geometry has changed, and there is a DNA-free side of the step (arrow). In Figure 5c, that space is beginning to fill, and the next step toward the left in the image (arrow) has a small amount of adsorbed DNA fragments. In Figure 5d, there seems to be a movement of the DNA to that step (arrow) meanwhile the terrace is getting smaller. In Figure 5e, only a small amount of DNA is left on the disappearing terrace edge, and an increasing amount of DNA is observed on the step edge to the left (arrows). In Figure 5f, the disappearing terrace is further dissolved and more than half of that step edge to the left is occupied by DNA. There is an empty section on the step edge (arrow) that has not yet been filled with DNA. In Figure 5g, the empty section is filled up by a DNA fragment, and only the upper part of the step edge is empty. In Figure 5h the step edge is filling up and there is a small section of the edge still free of DNA. In Figure 5i, it is evident that the step is now dissolving and DNA is building up on the dissolving terrace edge (arrow). We cannot determine if the DNA is getting increasingly fragmented because the fragments line up on the steps, exploiting the available space for adsorption. We observed no intact plasmids, even after exploring the surface after we disrupted the equilibrium, which supports that the binding does indeed facilitate fragmentation of the DNA.

3.4.2 | Quantification of the fragmentation

We confirmed DNA fragmentation as a result of calcite binding via bulk DNA extraction experiments. In the AFM experiments, we had a high surface-to-water volume (~1 cm (Hofreiter et al., 2003) surface and 40 μL liquid, and 1 ng plasmid DNA, with a further disequilibrium step by introducing 10 μL buffer). To quantify DNA adsorption, handle the extraction, and ensure mixing, we had a significantly lower surface-to-volume ratio in the bulk experiments. We added a double-stranded 1000 bp DNA fragment to calcite powder, and fragment analyzer smear analysis (35–750 bp and 750–1000 bp) of the extract showed a DNA extraction efficiency for calcite samples of ~93%, 90%, and 29%, respectively (Table S3). The extraction efficiency for positive control was ~78% and 98%. Of the total amount of DNA extracted, short fragments (<750 bp) accounted for 13%, 16%, and 10% for calcite samples (samples 1–3) and 0.2 and 0.8%, respectively, for the positive control (samples 6–7). These results suggest that most of the fragmentation happened on calcite, while only a small amount of fragmentation was caused by the extraction

FIGURE 5 Time sequence of desorption and re-adsorption of DNA fragments as the calcite surface dissolves. There is 10–30s between each frame.

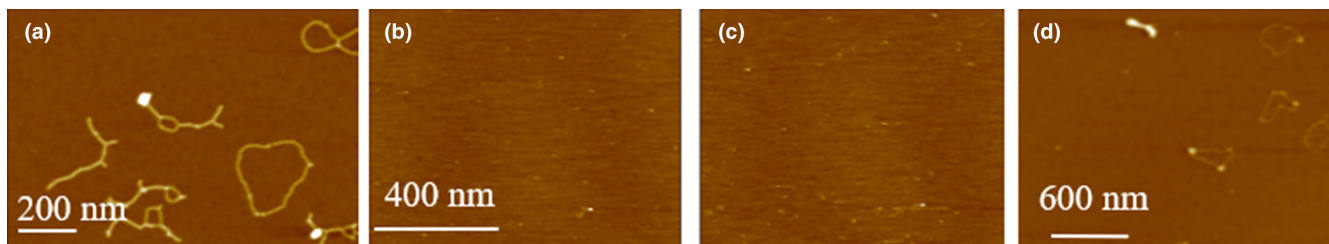
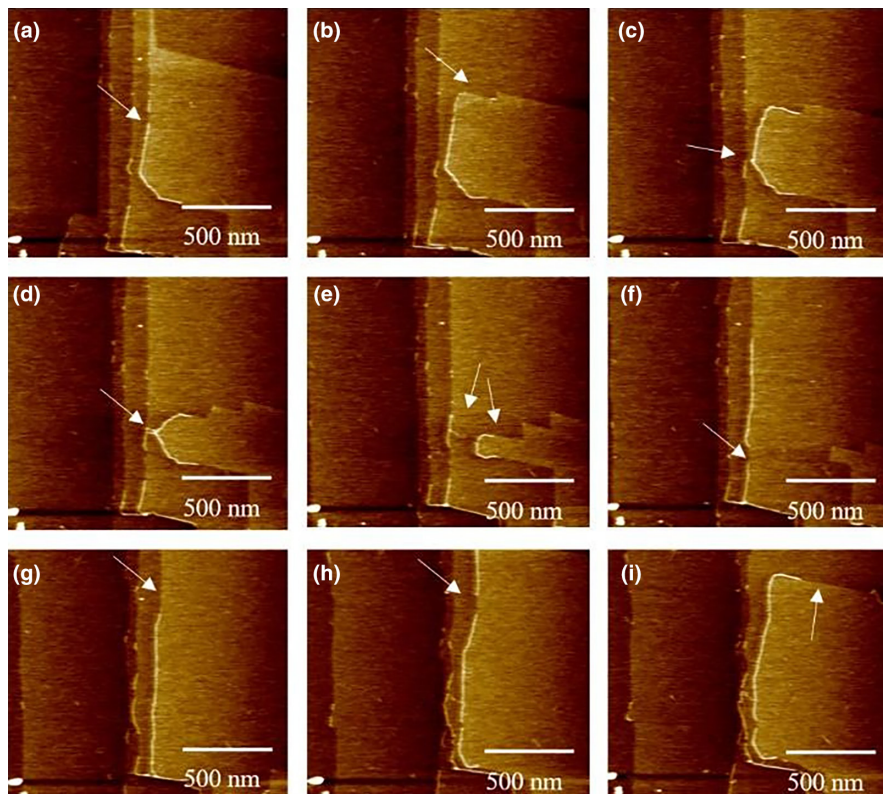


FIGURE 6 (a) Plasmid DNA adsorbed in ASW and imaged in liquid. (b) ASW added to the surface in a and imaged in the solution. (c) ASW liquid was exchanged for 1 mM CaCl_2 and imaged in the liquid. (d) The surface from c was dried and imaged in air.

process. In the AFM experiment, all the DNA images showed fragmentation. We ascribe the difference in fragmentation efficiency between the AFM and bulk experiments to the different solid-to-liquid ratio in the two setups. It should also be noted that AFM imaging does not provide a quantitative overview of the DNA, as we did not attempt to quantify the DNA adsorption, nor is it possible to image the surface in its entirety.

3.5 | Mobility of the adsorbed DNA on mica

The dynamics of DNA-mica interaction cannot be directly measured using AFM as the DNA is only weakly associated with the mica surface and hence easily displaced by the AFM tip. In order to use AFM for imaging, DNA molecules need to complex with mica via cations with a strong ionic potential, such as Ni^{2+} (Hansma & Laney, 1996). Regardless of the solution composition, drying the surface has proven to provide information on the conformation of the DNA

inherent to the adsorbing liquid composition (Zheng et al., 2003). We added plasmid DNA in artificial seawater (ASW) to a mica surface and imaged the DNA in air to confirm adsorption. The adsorbed plasmid molecules are arranged in a range of conformations (collapsed, circular, and coiled, Figure 6a). Adding ASW solution to the surface in Figure 6a and scanning the surface in the liquid, we were unable to detect circular plasmids (Figure 6b). Instead, we observe several small and mobile spots which highlight that the DNA is weakly associated with the mineral surface and the interaction strength is not high enough to draw the DNA to the surface allowing it to be imaged. Instead, the DNA is likely moved around by the AFM tip (as inferred by the striations observed in Figure 6b,c). Reducing the salinity and the cation charge density of the solution to 1 mM CaCl_2 , we are again unable to immobilize the DNA for imaging in the liquid and only observe mobile spots and striations (Figure 6c). Despite decreasing the ionic strength of the solutions as well as the charge density of the cations available, drying the surface and scanning it in the air revealed that the DNA did not fully desorb nor fragmented

the DNA. The adsorption dynamics confirm that most of the molecule was associated with the solution rather than with the surface while in liquid.

4 | DISCUSSION

Our results highlight that the adsorption process is an interplay between the adsorbed water layer, the charge density of the surface, surface topography, and the DNA charge. For the negatively charged mica surface, the ionic potential of the background ions plays a large role for the adsorbed DNA conformation. For calcite, the local charge density plays a role for the structuring of the associated water layer and the charge dense edge sites become the dominant sites for adsorption regardless of background ions. This behavior is characteristic for outer sphere and inner sphere adsorption, respectively. If, as in the case for mica, the DNA binds to the mineral through a cation bridge, the binding strength can be reduced by decreasing the concentration or the ionic potential of the solution. Such a change in solution conditions has been argued to essentially lead to desorption (Pastré et al., 2006; Thomson et al., 1996), and is unlikely to lead to fragmentation as also shown in Figure 6. In contrast, direct interaction between the DNA and the surface of calcite can create a strong association which becomes stronger with a decreased double layer (high ionic strength). For the specific case of the acute calcium step, the interaction is strong enough to break up the DNA helix and cause fragmentation of the molecule.

Through our experimental and simulation analyses, we determined that DNA's affinity for adsorption differs substantially between minerals such as mica and calcite, a finding pivotal for understanding DNA retention in both contemporary and historic sedimentary contexts. Specifically, while mica's DNA-binding potential largely hinges on solution composition, calcite would be highly likely to tightly bind DNA in any environment. The strong association with calcite suggests that calcite-adsorbed DNA is less likely to desorb if the composition of the background electrolyte is changed. In an open system such as soil or sediment, however, a change in solution composition would likely be followed by a shift in the calcite saturation state in the solution, which could lead to desorption and re-adsorption with severe consequences for DNA preservation. The binding to calcite step edges is shown here to induce fragmentation, and successions of de- and re-adsorption events would accelerate the fragmentation. In a cave environment where the calcite equilibrium can be maintained within a speleothem, any free DNA from a solution would have a higher chance of binding to the mineral surface. Even though, the initial binding of DNA to calcite conjures some strand fragmentation, the long-term stabilization of the strand in a relatively closed system (such as some stalagmites) would increase the potential for DNA preservation across timescales.

A holistic understanding of eDNA requires a synthesis of mineralogical and interfacial geochemical knowledge. Incorporating data from mineral-specific adsorption studies (mini-review in Sand

& Jelavić, 2018), alongside the present study's mechanistic insights, equips researchers to predict and comprehend DNA taphonomy more comprehensively. It becomes apparent that positively charged mineral surfaces will generally exhibit a higher affinity for DNA, while negatively charged surfaces, like nonclay silicates, might only weakly interact with DNA. When DNA molecules are weakly bound, most of the DNA molecule will be associated with the solution, likely leading to faster degradation by enzymatic activity, hydrolyses, and UV radiation, in contrast to a DNA molecule immobilized on a mineral surface through strong adsorption via numerous binding sites. Extrapolation to minerals such as clay minerals, which, in addition to the mica-like basal planes, can also contain positively charged edge sites. Adsorption to clay edge sites is very hard to investigate experimentally, and it is currently unclear if clay edge sites would induce fragmentation as seen for calcite. However, several studies have modeled the adsorption of nucleotides to clay edges (Mignon et al., 2019; Pedreira-Segade et al., 2016, 2018; Sand & Jelavić, 2018) and overall, for the purposes of estimating taphonomy, the edge sites can be expected to behave in a similar manner as the calcite edge sites in terms of binding affinity.

The variability in DNA preservation across diverse minerals and chemical contexts underscores the need for careful interpretation in any sedimentary DNA studies. For instance, comparing biodiversity measures from sedimentary profiles with alternating layers of mica and calcite (or minerals with varying degrees of DNA adsorption affinity) necessitates a nuanced understanding of DNA preservation dynamics in each layer. This complexity extends to interpreting DNA from various sedimentary sources, where the sediment's origin, travel path, and depositional environment all intertwine to influence DNA preservation and representation. As the field of eDNA progresses, new questions and challenges emerge. A comprehensive grasp of DNA preservation in sediments demands deeper insights into DNA-mineral associations across scales and DNA states (whole vs. fragmented). The research community must address significant knowledge gaps, including understanding the influence of other organic components on DNA preservation, discerning the thermodynamics and kinetics of DNA adsorption/desorption, and comprehending the degradation mechanisms of mineral-bound DNA. Regardless of these challenges, embracing mineralogy, interfacial geochemistry, and depositional environments will undoubtedly propel the eDNA field forward, refining our interpretations and broadening our scope of study.

5 | CONCLUSION AND RECOMMENDATIONS

Our results highlight that local mineral surface charge affects DNA adsorption. The interplay between DNA and background electrolyte becomes increasingly important for adsorption as the mineral surface charge decreases, such as for mica, suggesting ion bridging as an important adsorption mechanism. Additionally, a high positive surface charge density (calcite edges) facilitates the interaction

with the DNA molecule but also causes fragmentation of the double strand. Overall, the adsorbed conformation of the DNA is affected by both the adsorption process and the ionic potential of the background ions, in particular if the molecule adsorption is not confined to topographical or charge-dense sites but instead more freely to move on the surface.

Set in an environmental and depositional perspective, our data show that, (a) for negatively charged minerals such as mica, the environmental setting is vital for both the adsorption process and also for understanding (post)-depositional leakage and an important factor to take into account for determining DNA preservation in sediments and (b) for positively charged minerals such as calcite, DNA tends to be readily adsorbed and stably preserved over time and across diverse conditions, but only if the calcite maintains its equilibrium. Frequent disturbances in this equilibrium can lead to increased DNA fragmentation. Hence, fragmentation patterns offer more than just a glimpse of DNA's age; they can also indicate events that disrupt mineral solubility.

This research underscores the intertwined relationship between sediment mineralogy and both the prevailing and subsequent environmental conditions. Such intersections provide invaluable insights into the potential for DNA preservation in specific locales. It prompts us to reflect: Does the eDNA we extract mirror the mineralogical composition and environmental history of its deposit? And are we sufficiently informed about these interdependencies to interpret, for instance, historical biodiversity patterns?

AUTHOR CONTRIBUTIONS

CLF led and conducted the MD simulations and the MD interpretation and helped write the original manuscript. LD. conducted the AFM imaging, developed the experimental procedures associated and took part in the interpretations. OBAA made the CFM experiments, MZ led and conducted the extraction work. JQS contributed to the discussion and AFM work. MC provided context and helped draft the original manuscript. KKS conceptualized the study and designed the experimental work, interpreted the data and wrote the original manuscript.

ACKNOWLEDGMENTS

This work was supported by research grants from VILLUM FONDEN (00025352), the Danish Council for Independent Research (8123-00003A), and the Danish National Research Foundation (DNRF128). CLF acknowledges an EPSRC Programme Grant (grant EP/R018820/1) which funds the Crystallization in the Real World consortium. OBAA acknowledges funding from the European Union's Horizon 2020 research and innovation programme under the Marie Skłodowska-Curie grant agreement No. 892889. For the purpose of open access, MJC has applied a Creative Commons Attribution (CC BY) license to any Author Accepted Manuscript version arising from this submission.

CONFLICT OF INTEREST STATEMENT

None.

DATA AVAILABILITY STATEMENT

The data that support the findings of this study are available from the corresponding author upon reasonable request.

ORCID

K. K. Sand  <https://orcid.org/0000-0002-0720-7229>

REFERENCES

- Aschauer, U., Spagnoli, D., Bowen, P., & Parker, S. C. (2010). Growth modification of seeded calcite using carboxylic acids: Atomistic simulations. *Journal of Colloid and Interface Science*, 346(1), 226–231. <https://doi.org/10.1016/j.jcis.2010.02.057>
- Baker, A., Barnes, W. L., & Smart, P. L. (1996). Speleothem luminescence intensity and spectral characteristics: Signal calibration and a record of palaeovegetation change. *Chemical Geology*, 130(1), 65–76. [https://doi.org/10.1016/0009-2541\(96\)00003-4](https://doi.org/10.1016/0009-2541(96)00003-4)
- Brennan, E., & White, W. (2013). Luminescence of speleothems: A comparison of sources and environments. *Journal of Cave and Karst Studies*, 75(3), 211–217. <https://doi.org/10.4311/2012E50280>
- Butt, H.-J., & Jaschke, M. (1995). Calculation of thermal noise in atomic force microscopy. *Nanotechnology*, 6(1), 1–7. <https://doi.org/10.1088/0957-4484/6/1/001>
- Cooke, D. J., Gray, R. J., Sand, K. K., Stipp, S. L. S., & Elliott, J. A. (2010). Interaction of ethanol and water with the {101 $\bar{4}$ } surface of calcite. *Langmuir*, 26(18), 14520–14529. <https://doi.org/10.1021/la100670k>
- Cornell, W. D., Cieplak, P., Bayly, C. I., Gould, I. R., Merz, K. M., Ferguson, D. M., Spellmeyer, D. C., Fox, T., Caldwell, J. W., & Kollman, P. A. (1995). A second generation force field for the simulation of proteins, nucleic acids, and organic molecules. *Journal of the American Chemical Society*, 117(19), 5179–5197. <https://doi.org/10.1021/ja00124a002>
- De Yoreo, J. J., & Vekilov, P. G. (2003). Principles of crystal nucleation and growth. *Reviews in Mineralogy and Geochemistry*, 54(1), 57–93. <https://doi.org/10.2113/0540057>
- Dejean, T., Valentini, A., Duparc, A., Pellier-Cuit, S., Pompanon, F., Taberlet, P., & Miaud, C. (2011). Persistence of environmental DNA in freshwater ecosystems. *PLoS One*, 6(8), e23398. <https://doi.org/10.1371/journal.pone.0023398>
- Dhami, N. K., Mukherjee, A., & Watkin, E. L. J. (2018). Microbial diversity and mineralogical-mechanical properties of calcitic cave speleothems in natural and in vitro biomineralization conditions. *Frontiers in Microbiology*, 9, 40. <https://doi.org/10.3389/fmicb.2018.00040>
- Duguid, J. G., & Bloomfield, V. A. (1995). Aggregation of melted DNA by divalent metal ion-mediated cross-linking. *Biophysical Journal*, 69(6), 2642–2648. [https://doi.org/10.1016/S0006-3495\(95\)80134-7](https://doi.org/10.1016/S0006-3495(95)80134-7)
- Feuillie, C., Sverjensky, D. A., & Hazen, R. M. (2015). Attachment of ribonucleotides on α -alumina as a function of PH, ionic strength, and surface loading. *Langmuir*, 31(1), 240–248. <https://doi.org/10.1021/la504034k>
- Freeman, C. L., Harding, J. H., Cooke, D. J., Elliott, J. A., Lardge, J. S., & Duffy, D. M. (2007). New forcefields for modeling biomineralization processes. *Journal of Physical Chemistry C*, 111(32), 11943–11951. <https://doi.org/10.1021/jp071887p>
- Freeman, C. L., Asteriadis, I., Yang, M., & Harding, J. H. (2009). Interactions of organic molecules with calcite and magnesite surfaces. *Journal of Physical Chemistry C*, 113, 3666–3673.
- Freeman, C. L., Harding, J. H., Quigley, D., & Rodger, P. M. (2012). Protein binding on stepped calcite surfaces: Simulations of ovalocleidin-17 on calcite {31.16} and {31.8}. *Physical Chemistry Chemical Physics*, 14(20), 7287–7295. <https://doi.org/10.1039/C2CP23987F>
- Gale, J. D. (1997). GULP: A computer program for the symmetry-adapted simulation of solids. *Journal of the Chemical Society, Faraday Transactions*, 93(4), 629–637. <https://doi.org/10.1039/A606455H>

- Geissbühler, P., Fenter, P., DiMasi, E., Srajer, G., Sorensen, L. B., & Sturchio, N. C. (2004). Three-dimensional structure of the calcite-water interface by surface X-ray scattering. *Surface Science*, 573(2), 191–203. <https://doi.org/10.1016/j.susc.2004.09.036>
- Giguet-Covex, C., Ficetola, G. F., Walsh, K., Poulenard, J., Bajard, M., Fouinat, L., Sabatier, P., Gielly, L., Messenger, E., Develle, A. L., David, F., Taberlet, P., Brisset, E., Guiter, F., Sinet, R., & Arnaud, F. (2019). New insights on lake sediment DNA from the catchment: Importance of taphonomic and analytical issues on the record quality. *Scientific Reports*, 9(1), 14676. <https://doi.org/10.1038/s41598-019-50339-1>
- Greaves, M. P., & Wilson, M. T. (1969). The adsorption of nucleic acids by montmorillonite. *Soil Biology and Biochemistry*, 1(4), 317–323. [https://doi.org/10.1016/0038-0717\(69\)90014-5](https://doi.org/10.1016/0038-0717(69)90014-5)
- Haile, J., Holdaway, R., Oliver, K., Bunce, M., Gilbert, M. T. P., Nielsen, R., Munch, K., Ho, S. Y. W., Shapiro, B., & Willerslev, E. (2007). Ancient DNA chronology within sediment deposits: Are paleobiological reconstructions possible and is DNA leaching a factor? *Molecular Biology and Evolution*, 24(4), 982–989. <https://doi.org/10.1093/molbev/msm016>
- Hansma, H. G., & Laney, D. E. (1996). DNA binding to mica correlates with cationic radius: Assay by atomic force microscopy. *Biophysical Journal*, 70(4), 1933–1939.
- Hofreiter, M., Mead, J. I., Martin, P., & Poinar, H. N. (2003). Molecular caving. *Current Biology*, 13(18), R693–R695. <https://doi.org/10.1016/j.cub.2003.08.039>
- Hutter, J. L., & Bechhoefer, J. (1993). Calibration of atomic-force microscope tips. *The Review of Scientific Instruments*, 64(7), 1868–1873. <https://doi.org/10.1063/1.1143970>
- Israelachvili, J. N. (Ed.). (2011). *Intermolecular and surface forces* (3rd ed., p. iii). Academic Press. <https://doi.org/10.1016/B978-0-12-375182-9.10025-9>
- Jelavić, S., Mitchell, A. C., & Sand, K. K. (2020). Fate of organic compounds during transformation of ferrihydrite in iron formations. *Geochemical Perspectives Letters*, 15, 25–29. <https://doi.org/10.7185/geochemlet.2030>
- Jelavić, S., Nielsen, A. R., Stipp, S. L. S., & Bovet, N. (2018). Composition in the interface between clay mineral surfaces and divalent cation electrolytes. *Langmuir*, 34(24), 7011–7020. <https://doi.org/10.1021/acs.langmuir.8b00370>
- Kester, D. R., Duedall, I. W., Connors, D. N., & Pytkowicz, R. M. (1967). Preparation of artificial Seawater1. *Limnology and Oceanography*, 12(1), 176–179. <https://doi.org/10.4319/lo.1967.12.1.0176>
- Kjær, K. H., Winther Pedersen, M., De Sanctis, B., De Cahsan, B., Korneliusen, T. S., Michelsen, C. S., Sand, K. K., Jelavić, S., Ruter, A. H., Schmidt, A. M. A., Kjeldsen, K. K., Tesakov, A. S., Snowball, I., Gosse, J. C., Alsos, I. G., Wang, Y., Dockter, C., Rasmussen, M., Jørgensen, M. E., ... Willerslev, E. (2022). A 2-million-year-old ecosystem in Greenland uncovered by environmental DNA. *Nature*, 612(7939), 283–291. <https://doi.org/10.1038/s41586-022-05453-y>
- Kosmulski, M. (2009). *Surface charging and points of zero charge*. Routledge & CRC Press. <https://www.routledge.com/Surface-Charging-and-Points-of-Zero-Charge/Kosmulski/p/book/9780367577346>
- Lee, S. S., Fenter, P., Park, C., Sturchio, N. C., & Nagy, K. L. (2010). Hydrated cation speciation at the muscovite (001)–water interface. *Langmuir*, 26(22), 16647–16651. <https://doi.org/10.1021/la1032866>
- Levy-Booth, D. J., Campbell, R. G., Gulden, R. H., Hart, M. M., Powell, J. R., Klironomos, J. N., Pauls, K. P., Swanton, C. J., Trevors, J. T., & Dunfield, K. E. (2007). Cycling of extracellular DNA in the soil environment. *Soil Biology and Biochemistry*, 39(12), 2977–2991. <https://doi.org/10.1016/j.soilbio.2007.06.020>
- Lu, N., Zilles, J. L., & Nguyen, T. H. (2010). Adsorption of extracellular chromosomal DNA and its effects on natural transformation of *Azotobacter vinelandii*. *Applied and Environmental Microbiology*, 76(13), 4179–4184. <https://doi.org/10.1128/AEM.00193-10>
- Maity, S., Zanut, D., Razvag, Y., Das, P., Alemán, C., & Reches, M. (2015). Elucidating the mechanism of interaction between peptides and inorganic surfaces. *Physical Chemistry Chemical Physics*, 17(23), 15305–15315. <https://doi.org/10.1039/C5CP00088B>
- Mendoza, M. L. Z., Lundberg, J., Ivarsson, M., Campos, P., Nylander, J. A. A., Sallstedt, T., & Dalen, L. (2016). Metagenomic analysis from the interior of a speleothem in Tjuv-Ante's cave, northern Sweden. *PLoS One*, 11(3), e0151577. <https://doi.org/10.1371/journal.pone.0151577>
- Michalkova, A., Robinson, T. L., & Leszczynski, J. (2011). Adsorption of thymine and uracil on 1:1 clay mineral surfaces: Comprehensive ab initio study on influence of sodium cation and water. *Physical Chemistry Chemical Physics*, 13(17), 7862–7881. <https://doi.org/10.1039/C1CP00008J>
- Mignon, P., Navarro-Ruiz, J., Rimola, A., & Sodupe, M. (2019). Nucleobase stacking at clay edges, a favorable interaction for RNA/DNA oligomerization. *ACS Earth and Space Chemistry*, 3(6), 1023–1033. <https://doi.org/10.1021/acsearthspacechem.9b00021>
- Murugesapillai, D., Bouaziz, S., James Maher, L., Israeloff, N. E., Cameron, C. E., & Williams, M. C. (2017). Accurate nanoscale flexibility measurement of DNA and DNA-protein complexes by atomic force microscopy in liquid. *Nanoscale*, 9(31), 11327–11337. <https://doi.org/10.1039/C7NR04231K>
- Nguyen, T. H., & Chen, K. L. (2007). Role of divalent cations in plasmid DNA adsorption to natural organic Matter-coated silica surface. *Environmental Science & Technology*, 41(15), 5370–5375. <https://doi.org/10.1021/es070425m>
- Pastré, D., Hamon, L., Landousy, F., Sorel, I., David, M.-O., Zozime, A., Le Cam, E., & Piétrement, O. (2006). Anionic polyelectrolyte adsorption on mica mediated by multivalent cations: A solution to DNA imaging by atomic force microscopy under high ionic strengths. *Langmuir*, 22(15), 6651–6660. <https://doi.org/10.1021/la053387y>
- Pedersen, M. W., Ruter, A., Schweger, C., Friebe, H., Staff, R. A., Kjeldsen, K. K., Mendoza, M. L. Z., Beaudoin, A. B., Zutter, C., Larsen, N. K., Potter, B. A., Nielsen, R., Rainville, R. A., Orlando, L., Meltzer, D. J., Kjær, K. H., & Willerslev, E. (2016). Postglacial viability and colonization in North America's ice-free corridor. *Nature*, 537(7618), 45–49. <https://doi.org/10.1038/nature19085>
- Pedreira-Segade, U., Feuillie, C., Pelletier, M., Michot, L. J., & Daniel, I. (2016). Adsorption of nucleotides onto ferromagnesian phyllosilicates: Significance for the origin of life. *Geochimica et Cosmochimica Acta*, 176, 81–95. <https://doi.org/10.1016/j.gca.2015.12.025>
- Pedreira-Segade, U., Hao, J., Razafitianamaharavo, A., Pelletier, M., Marry, V., Le Crom, S., Michot, L. J., & Daniel, I. (2018). How do nucleotides adsorb onto clays? *Life*, 8(4), 59. <https://doi.org/10.3390/life8040059>
- Raiteri, P., & Gale, J. D. (2010). Water is the key to nonclassical nucleation of amorphous calcium carbonate. *Journal of the American Chemical Society*, 132(49), 17623–17634. <https://doi.org/10.1021/ja108508k>
- Sader, J. E., Sanelli, J. A., Adamson, B. D., Monty, J. P., Wei, X., Crawford, S. A., Friend, J. R., Marusic, I., Mulvaney, P., & Bieske, E. J. (2012). Spring constant calibration of atomic force microscope cantilevers of arbitrary shape. *The Review of Scientific Instruments*, 83(10), 103705. <https://doi.org/10.1063/1.4757398>
- Saeki, K., Sakai, M., & Wada, S.-I. (2010). DNA adsorption on synthetic and natural allophanes. *Applied Clay Science*, 50(4), 493–497. <https://doi.org/10.1016/j.clay.2010.09.015>
- Sand, K. K., & Jelavić, S. (2018). Mineral facilitated horizontal gene transfer: A new principle for evolution of life? *Frontiers in Microbiology*, 9, 2217. <https://doi.org/10.3389/fmicb.2018.02217>
- Sand, K. K., Yang, M., Makovicky, E., Cooke, D. J., Hassenkam, T., Bechgaard, K., & Stipp, S. L. S. (2010). Binding of ethanol on calcite: The role of the OH bond and its relevance to biomineralization. *Langmuir*, 26(19), 15239–15247. <https://doi.org/10.1021/la101136j>
- Seersholm, F. V., Pedersen, M. W., Sjøe, M. J., Shokry, H., Mak, S. S. T., Ruter, A., Raghavan, M., Fitzhugh, W., Kjær, K. H., Willerslev, E.,

- Meldgaard, M., Kapel, C. M. O., & Hansen, A. J. (2016). DNA evidence of bowhead whale exploitation by Greenlandic Paleo-Inuit 4,000 years ago. *Nature Communications*, 7(1), 13389. <https://doi.org/10.1038/ncomms13389>
- Selkoe, K. A., Gaggiotti, O. E., Treml, E. A., Wren, J. L. K., Donovan, M. K., & Toonen, R. J. (1829). The DNA of coral reef biodiversity: Predicting and protecting genetic diversity of reef assemblages. *Proceedings of the Royal Society B: Biological Sciences*, 2016(283), 20160354. <https://doi.org/10.1098/rspb.2016.0354>
- Slon, V., Hopfe, C., Weiß, C. L., Mafessoni, F., de la Rasilla, M., Lalueza-Fox, C., Rosas, A., Soressi, M., Knul, M. V., Miller, R., Stewart, J. R., Derevianko, A. P., Jacobs, Z., Li, B., Roberts, R. G., Shunkov, M. V., de Lumley, H., Perrenoud, C., Gušić, I., ... Meyer, M. (2017). Neandertal and Denisovan DNA from Pleistocene sediments. *Science*, 356(6338), 605–608. <https://doi.org/10.1126/science.aam9695>
- Smith, W., & Forester, T. R. (1996). DL_POLY_2.0: A general-purpose parallel molecular dynamics simulation package. *Journal of Molecular Graphics*, 14(3), 136–141. [https://doi.org/10.1016/S0263-7855\(96\)00043-4](https://doi.org/10.1016/S0263-7855(96)00043-4)
- Spagnoli, D., Kerisit, S., & Parker, S. C. (2006). Atomistic simulation of the free energies of dissolution of ions from flat and stepped calcite surfaces. *Journal of Crystal Growth*, 294(1), 103–110. <https://doi.org/10.1016/j.jcrysgro.2006.05.030>
- Sparks, D. J., Romero-González, M. E., El-Taboni, E., Freeman, C. L., Hall, S. A., Kakonyi, G., Swanson, L., Banwart, S. A., & Harding, J. H. (2015). Adsorption of poly acrylic acid onto the surface of calcite: An experimental and simulation study. *Physical Chemistry Chemical Physics*, 17(41), 27357–27365. <https://doi.org/10.1039/C5CP00945F>
- Stahlschmidt, M. C., Collin, T. C., Fernandes, D. M., Bar-Oz, G., Belfer-Cohen, A., Gao, Z., Jakeli, N., Matskevich, Z., Meshveliani, T., Pritchard, J. K., McDermott, F., & Pinhasi, R. (2019). Ancient mammalian and plant DNA from late quaternary stalagmite layers at Solkoto cave, Georgia. *Scientific Reports*, 9(1), 6628. <https://doi.org/10.1038/s41598-019-43147-0>
- Thomsen, P. F., Kielgast, J., Iversen, L. L., Møller, P. R., Rasmussen, M., & Willerslev, E. (2012). Detection of a diverse marine fish Fauna using environmental DNA from seawater samples. *PLoS One*, 7(8), e41732. <https://doi.org/10.1371/journal.pone.0041732>
- Thomson, N. H., Kasas, S., Smith Hansma, H. G., & Hansma, P. K. (1996). Reversible binding of DNA to mica for AFM imaging. *Langmuir*, 12(24), 5905–5908. <https://doi.org/10.1021/la960497j>
- Vuillemin, A., Horn, F., Alawi, M., Henny, C., Wagner, D., Crowe, S. A., & Kallmeyer, J. (2017). Preservation and significance of extracellular DNA in ferruginous sediments from Lake Towuti, Indonesia. *Frontiers in Microbiology*, 8, 8.
- Watson, G. W., Kelsey, E. T., de Leeuw, N. H., Harris, D. J., & Parker, S. C. (1996). Atomistic simulation of dislocations, surfaces and interfaces in MgO. *Journal of the Chemical Society, Faraday Transactions*, 92(3), 433–438. <https://doi.org/10.1039/FT9969200433>
- Yang, M., Stipp, S. L. S., & Harding, J. (2008). Biological control on calcite crystallization by polysaccharides. *Crystal Growth & Design*, 8(11), 4066–4074. <https://doi.org/10.1021/cg800508t>
- Ye, M., Li, B., Zhang, Y., Li, H., Wang, X., & Hu, J. (2011). Confined water nanofilm promoting nonenzymatic degradation of DNA molecules. *The Journal of Physical Chemistry. B*, 115(12), 2754–2758. <https://doi.org/10.1021/jp109212d>
- Yu, W. H., Li, N., Tong, D. S., Zhou, C. H., Lin (Cynthia), C. X., & Xu, C. Y. (2013). Adsorption of proteins and nucleic acids on clay minerals and their interactions: A review. *Applied Clay Science*, 80–81, 443–452. <https://doi.org/10.1016/j.clay.2013.06.003>
- Zhai, H., Wang, L., & Putnis, C. V. (2019). Molecular-scale investigations reveal noncovalent bonding underlying the adsorption of environmental DNA on mica. *Environmental Science & Technology*, 53(19), 11251–11259. <https://doi.org/10.1021/acs.est.9b04064>
- Zheng, J., Li, Z., Wu, A., & Zhou, H. (2003). AFM studies of DNA structures on mica in the presence of alkaline earth metal ions. *Biophysical Chemistry*, 104(1), 37–43. [https://doi.org/10.1016/s0301-4622\(02\)00335-6](https://doi.org/10.1016/s0301-4622(02)00335-6)
- Zhu, B., Xu, X., & Tang, R. (2013). Hydration layer structures on calcite facets and their roles in selective adsorptions of biomolecules: A molecular dynamics study. *The Journal of Chemical Physics*, 139(23), 234705. <https://doi.org/10.1063/1.4848696>

SUPPORTING INFORMATION

Additional supporting information can be found online in the Supporting Information section at the end of this article.

How to cite this article: Freeman, C. L., Dieudonné, L., Agbaje, O. B. A., Žure, M., Sanz, J. Q., Collins, M., & Sand, K. (2023). Survival of environmental DNA in sediments: Mineralogic control on DNA taphonomy. *Environmental DNA*, 00, 1–15. <https://doi.org/10.1002/edn3.482>